Charles University, Prague
Faculty of Mathematics and Physics

THE STUDY OF INSTABILITIES IN SOLAR WIND AND IN MAGNETOSHEATH AND THEIR INTERACTION WITH THE EARTH'S MAGNETOSPHERE

Abstract of Doctoral Thesis

Kateřina Andréeová

Department of Surface and Plasma Science
V Holešovičkách 2, 180 00 Praha 8

Study branch: f2 – Physics of Plasmas and Ionized Media

Supervisor: Doc. RNDr. Lubomír Přech, Dr.

Prague, July 2008

Univerzita Karlova v Praze
Matematicko–fyzikální fakulta

STUDIUM NESTABILIT VE SLUNEČNÍM VĚTRU A PŘECHODOVÉ OBLASTI A JEJICH INTERAKCE S MAGNETOSFÉROU ZEMĚ

Autoreferát disertační práce

Kateřina Andréeová

Katedry fyziky povrchů a plazmatu
V Holešovičkách 2, 180 00 Praha 8

Obor: f2 – Fyzika plazmatu a ionizovaných prostředí

Školitel: Doc. RNDr. Lubomír Přech, Dr.

Praha, červenec 2008

Disertační práce byla vypracována na základě výsledků vědecké práce na Katedře fyziky plazmatu a ionizovaných prostředív letech 2004–2008 během mého doktorandského studia na Matematicko-fyzikální fakultě Univerzity Karlovy v Praze.

Uchazeč:
Mgr. Kateřina Andréeová
Katedra fyziky povrchů a plazmatu MFF UK
V Holešovičkách 2
180 00 Praha 8

Školitel:
Doc. RNDr. Lubomír Přech, Dr.
Katedra fyziky povrchů a plazmatu MFF UK
V Holešovičkách 2
180 00 Praha 8

Oponenti:
Mgr. Andriy Koval, Ph.D.
NASA Goddard Space Flight Center
Greenbelt, Maryland MD 20705
USA

Doc. RNDr. Marian Karlický, DrSc.
Astronomický ústav AV ČR
Fričova 298
251 65 Ondřejov

Autoreferát byl rozeslán dne 2008

Obhajoba se koná dne 30. září 2008 v 10.45 hodin před komisí pro obhajoby doktorských prací v oboru f2, Fyzika plazmatu a ionizovaných prostředí, na MFF UK, V Holešovičkách 2, 180 00 Praha 8, v místnosti A042.

S disertací je možno se seznámit na Útvaru doktorského studia MFF UK, Ke Karlovu 3, 121 16 Praha 2.

Předsedkyně RDSO f2: Prof. RNDr. Jana Šafránová, DrSc.

Introduction

Interplanetary shocks (IPS) represent structures which can propagate in the solar wind and into the Earth's magnetosphere and interact with it. One of the results are magnetosphere compressions/expansions and magnetopause and tail modification. On the ground these processes are related to geomagnetic phenomena called sudden commencements/sudden impulses. In comparison to other IPS, fast forward shocks are stronger, have higher occurrence in the solar wind, and cause more intense compression of the Earth's magnetosphere, so they are preferential subjects of our study. The fast forward shocks are usually connected with the fast stream interfaces of the corotating interaction regions or they are precursors of the large and fast coronal ejecta - flares and magnetic clouds.

Interaction of fast forward shocks with the bow shock and magnetopause

The interplanetary fast forward shocks usually cause an intense compression of the Earth's magnetosphere(see Figure 1). These type of shocks propagate in the solar wind plasma frame with a speed about 50–200 km/s [Berdichevsky et al., 2000].

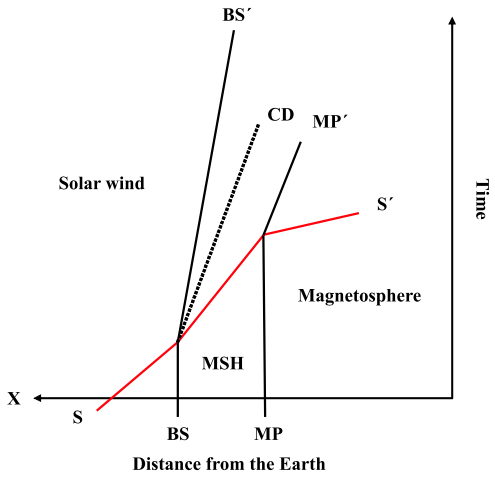

Figure 1: Schematic plot of interaction between the fast shock (FS) and the bow shock (BS) and magnetopause (MP). X axis depicts distance from the Earth (Sun–Earth line) and Y axis depicts time. Perpendicular lines show initial position of BS and MP. Oblique lines show the earthward motion (compressions of BS and MP and propagation of FS/disturbance into the magnetosphere) of the structures. MSH ≡ magnetosheath. CD ≡ contact discontinuity. S or S' ≡ shock. Adapted from Yan and Lee [1996].

The modification of the shock inside the Earth's magnetosphere has been studied by several authors using gas dynamic and magnetohydrodynamic modeling or using the Rankine–Hugoniot conditions, such as Spreiter and Stahara [1994], Grib et al. [1979], Grib [1982], and Zhuang et al. [1981]. Magnetohydrodynamic modeling of the interaction between the Earth's bow shock and the IP shocks or rotational discontinuities has been performed by Yan and Lee [1996]. Considering shock planarity in the solar wind, the front of the shocks may be curved near the flank magnetopause, as shown by Koval

et al. [2005, 2006]. The IP shock propagation along a normal direction has been also studied by Villante et al. [2004]. They found a time delay of about 5 minutes from the bow shock to the ground for almost radially propagating structures. They also estimated the speed of the shock in the magnetosheath to be $\sim 1/3 - \sim 1/4$ of the shock speed in the solar wind. Interaction of the FFS with the bow shock creates a train of discontinuities behind fast forward shock. It moves with a similar speed in the magnetosphere (see local 3D MHD simulation results by Samsonov et al. [2006]). In the magnetosheath, such compound discontinuity was described by Šafránková et al. [2007a] and its speed determined in a case study by Prech et al. [2008].

The analysis of Rankine-Hugoniot conditions performed by Grib et al. [1979] shows that interactions of FFS with the magnetopause result in a rarefaction waves propagating toward the bow shock [Zhuang et al., 1981].

According to global numerical MHD simulation performed by Guo et al. [2005] the shock orientation plays an important role in determining the IP shock-magnetosphere interaction effects. They compared the IP shocks with the same solar wind dynamic pressure and IMF B_z but with the different direction of propagation, parallel and oblique to the Sun-Earth line. In the first case, observation at geostationary orbit at local noon showed that the front of the magnetic field compression lasted about 1 min. The ramp may be split in two parts with a small decrease in between. A similar jump existed in the oblique case but lasted 5 minute.

Tamao [1964] found that isotropic compressional hydromagnetic wave are generated at the magnetopause, starting at a single point of the first contact but later the source is moving with the IP shock/magnetopause interaction region, that are propagating inward through the magnetosphere. In the case study Wilken et al. [1982] estimated propagation velocities to be about 600 km/s in the radial direction (from the geostationary orbit to the ground) and about 910 km/s in the azimuthal direction in the geostationary orbit plane. Nopper et al. [1982] estimated impulse disturbance speed about 1500 km/s within the geostationary orbit.

The aims of the thesis

The aims of this thesis are to study different types of interplanetary shocks in the solar wind, their propagation into the Earth's magnetosphere, and their modifications. We have chosen fast forward shocks because of their higher occurrence in the solar wind and as precursors of the arrival of large solar wind structures from the Sun, such as CMEs and CIRs.

In the thesis, we discuss following topics:

- Interaction of the interplanetary fast forward shocks with the Earth's bow shock.
- Statistical analysis of the fast forward shock speed in different parts of the Earth's magnetosphere, including a short statistical study to discuss the fast forward shock properties and dependencies on the different solar wind parameters.
- Detailed investigation of two close interplanetary shocks propagating through the magnetosphere.
- Comparison of these observations with results of MHD modeling of the same events.

- Short comparison of two MHD simulation tool results modeling the event.

Data set

We have selected FFS events from the interplanetary shock database compiled by Kasper [2005] and the SOHO [2007] database.

For investigation of the interaction of the IPS with the Earth's magnetosphere, we have used simultaneous plasma and magnetic field data from Wind [Lepping et al., 1995; Ogilvie et al., 1995; Lin et al., 1995], IMP-8 magnetic field (http://nssdcftp.gsfc. nasa.gov/spacecraft_data/imp/imp8/mag/ (A. Szabo and R. P. Lepping, NASA GSFC)) and plasma instruments [Bellomo and Mavretic, 1978], SOHO [Ipavich et al., 1998], ACE [Smith et al., 1998; McComas et al., 1998], Interball-1 [Klimov et al., 1997; Nozdrachev et al., 1998; Safrankova et al., 1997], Geotail [Kokubun et al., 1994; Mukai et al., 1994], Cluster [Balogh et al., 1997; Reme et al., 1997], GOES-8 to GOES-12 [Singer et al., 1996], and Polar [Russell et al., 1995; Harvey et al., 1995] in the solar wind, in the magnetosheath, and in the magnetosphere. Some data were provided also by the Genesis, Double Star TC1, and geostationary LANL satellites. The satellite data were mainly obtained through the CDAWeb service (http://cdaweb.gsfc.nasa.gov) or the project-dedicated archives (Cluster Active Archive http://caa.estec.esa.int/, DARTS http:// www.darts.isas.ac.jp/stp/geotail/, CNES-SADS http://sads.cnes.fr:8010/).

During our analysis, we assumed FFS as planar shocks with the constant speed in the solar wind. We calculated shock normals using different methods (RH or 4 S/C), and from the multi-spacecraft timing we calculated disturbance speeds in the Earth's magnetosphere. We compared the results with existing MHD simulations and also run own simulation aimed to the comparison with the real events.

Results

Interaction of the IP shock with both the bow shock and magnetopause

In the papers by Šafránková et al. [2007b,a], we investigated the evolution of IP shocks through the magnetospheric boundaries in the magnetosheath. We analyzed several observations of IP shocks in the magnetosheath and compared them to results of a local MHD model [Samsonov et al., 2006] and discussed global features of the IP shock-bow shock-magnetopause interaction as well as the structure of the IP shock front. From our detailed analysis based on the Interball-1 observations, we concluded that:

1. the IP shock passage into the magnetosheath causes the inward motion of the bow shock as a result of changes of parameters downstream of the IP shock, as predicted also by Rankine-Hugoniot conditions (e.g., Grib et al. [1979]; Zhuang et al. [1981]);

2. the inward bow shock motion is followed by an opposite motion and a combination of these two displacements creates a bow shock indentation [Šafránková et al., 2007a] that moves along the bow shock surface with the IP shock; it is often identified as two bow shock crossings in observations;

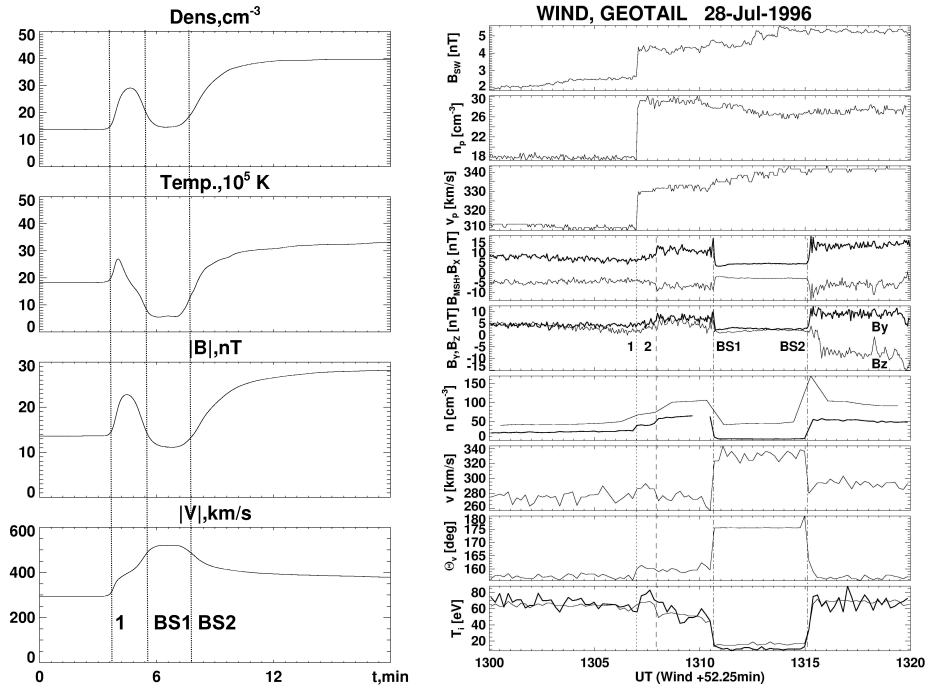

(a) (b)

Figure 2: (a) Simulated profiles of the density, temperature, magnetic field magnitude, and velocity. The vertical lines denote IP shock (1), bow shock crossings BS1 and BS2. (b) Wind observation of the interplanetary shock on July 28, 1996 (first three panels), together with Geotail observation in the magnetosheath (six lower panels). Panels from top: solar wind magnetic field magnitude B_{SW}, the solar wind density n_p and velocity v_p in GSE coordinates, next two panels showing magnetic field B_{MSH}, B_X, and B_Y, B_Z, density n, velocity v in the magnetosheath, cone angle Θ_v, and ion temperature T. The shock parameters in the solar wind are $v_{sh} = 339$ km/s, $M_A = 2.06$, and $n = [-0.92, -0.06, -0.39]$.

3. the interaction of IP shock and bow shock frequently causes a splitting of the IP shock front into two steps (similarly as in 1-D MHD simulations of Yan and Lee [1996])with an usual time lag of the order of one minute. Furthermore, the authors note that these two observed discontinuities having very similar velocities are generally consistent with the MHD magnetosheath model of Samsonov et al. [2006].

As an example of this comparison of observations with MHD predictions, we present here one event that was observed on July 28, 1996 by Geotail. In the Samsonov et al. [2006] model, we put an artificial spacecraft on the Z_{GSM} axis near the bow shock and the predicted profiles of basic parameters are plotted in Figure 2a for a run with a standing magnetopause. The spacecraft would observe the IP shock in the magnetosheath and then it would cross the bow shock because of its inward motion. The modification of the magnetosheath parameters by the reverse shock reflected from the standing magnetopause results in the bow shock outward motion that is recorded as a consecutive bow shock crossing.

The IP shock observations in the magnetosheath is shown in Figure 2b. The shock was registered by Wind at 1214 UT on July 28, 1996. We note that the predicted time of

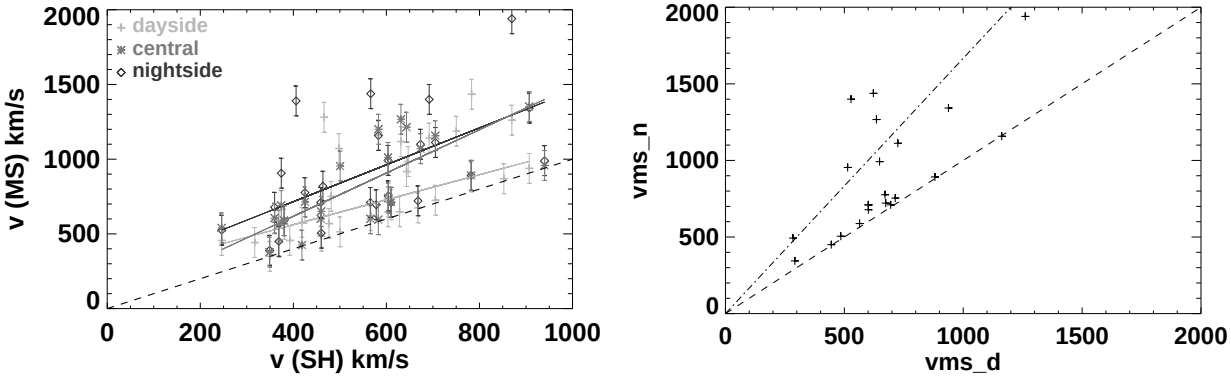

(a) (b)

Figure 3: (a) Relation of the disturbance speed in the Earths magnetosphere to the shock speed in the solar wind black color denotes dayside values, grey trans-terminator (central) values and light grey - nightside values. Light grey, grey and black lines show linear fits of these dependencies. Disturbance speed is higher in the Earths magnetosphere than in the solar wind and higher in the nightside than in the dayside magnetosphere.(b) Dependence of nightside disturbance speed on dayside disturbance speed. Dashed line depicts ratio 1:1 and means lower limit. Observations above the line show that speeds gradually increase from the dayside to the nightside region.

the shock propagation from Wind to Geotail was 50 min, whereas that observed was 52 min.

Statistical analysis

According to our study [Andreeova and Prech, 2007b] [A1] the speed of waves in the Earth's magnetosphere are higher than the original shock speed in the solar wind (see Figure 3a). We studied disturbance speeds in the different regions of the magnetosphere, dayside, central and nightside, as shown in Figure 3a. According to this, the disturbance speeds gradually increase from the dayside to the nightside (Figure 3b).

The compression ratio, defined as the ratio of downstream and upstream density, and dynamic pressure, see Figure 4a, are attributes which describe the shock strength. The observed magnetospheric speeds decrease for smaller values of the dynamic pressure (less than 2.5 nPa) and start to increase for higher values.

Case study: November 9, 2002

On November 9, 2002 (Table 1, 2), the Wind satellite observed two interplanetary shocks in sequence after 1724 UT and 1827 UT. The corresponding components of the shock normal vector were (-0.99, 0.15, -0.05) and (-0.98, -0.03, -0.20) in the GSE system. The θ_{Bn} angle was $\sim 43^{\circ}$ and 70°, the compression ratio 1.69 and 2.01, respectively.

The IMF was Parker-spiral-like and B_Z was positive both upstream and downstream of these events ($\theta \approx 30 - 60^{\circ}, \phi \approx 130^{\circ}$). The situation is depicted in Figure 5a,b for the two events. During that time, the satellites SOHO, ACE, Genesis, and Geotail were also operating in the solar wind, while the geosynchronous GOES–8 and GOES–10 satellites

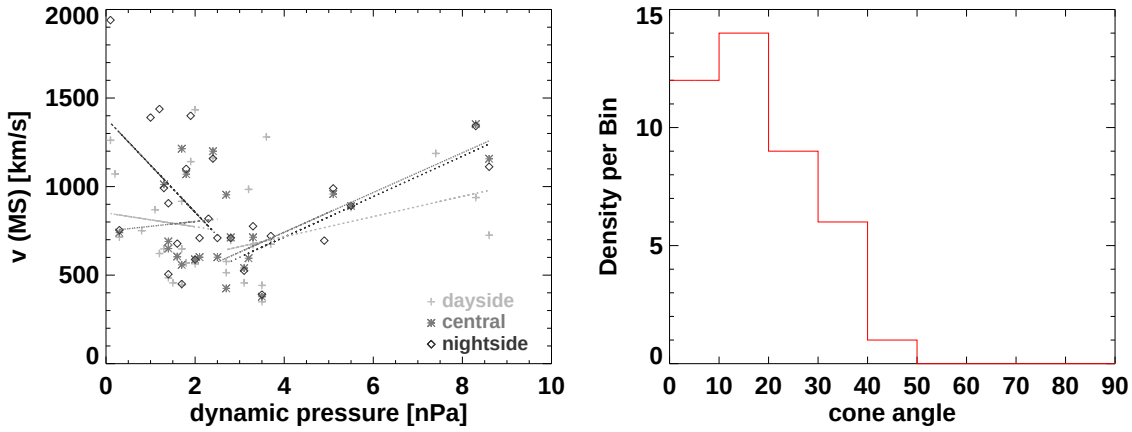

(a) (b)

Figure 4: (a) Dependence of the disturbance speed on the dynamic pressure upstream of the IP shock. Dashed color lines depict linear fits of these dependencies. (b) Distribution of cone angles of the shock normal (0-90 degrees) for the events in our data set. The cone angle of a shock perpendicular to the Sun-Earth line is 0 degree, the cone angle equal to 90 degrees corresponds to a shock parallel to the Sun-Earth line. Fast forward shocks propagate almost quasi-perpendicular to Sun-Earth line.

were in the Earth's magnetosphere. The Cluster spacecraft constellation was situated on the night side in the dusk flank plasma sheet near the magnetopause before the events. It orbited behind the quasiperpendicular part of the bow shock, so we don't expect any foreshock effects there.

For the two FF shocks, we calculated speeds of corresponding disturbances inside the Earth's magnetosphere between pairs of satellites along the original shock normal direction. Calculated speeds of disturbances were higher in the Earth's magnetosphere than in the solar wind (Andreeova and Prech [2007a]) [A1], see Figure 5a,b. Speeds of the disturbances in the magnetosphere calculated from MP to GOES 8, 10 were for the first event 550-580 km/s and for the second event 670 km/s, from the dayside to the nightside magnetosphere for the first event 580-590 km/s and for the second event 710-760 km/s, and between Cluster and Polar in the nightside for the first event 590 km/s and for the second event 780 km/s. The speed of the disturbances gradually increased from the dayside to the tail. Our results generally agree with estimates by Wilken et al. [1982] and Nopper et al. [1982](about 600–1500 km/s): our compressional front speeds are similar to their lower values representing the radial inward motion, but are smaller than their values for the azimuthal/near-geostationary-orbit propagation. The difference may be caused by a diverse state of the magnetosphere and content of plasma (mainly the density of plasma near and outside the geostationary orbit): in the Wilken et al. [1982] case, the preshock magnetopause had been already compressed near to the geosynchronous orbit (subsolar magnetopause at about $R_0 \sim 7.8\ R_{\rm E}$). Likewise, we got higher speed for the second event when the magnetopause was initially closer to the Earth ($R_0 \sim 9.7\ R_{\rm E}$) than before the first event ($R_0 \sim 11.7\ R_{\rm E}$). We also got slightly higher values for the propagation speed to Cluster (significant at least in the second event) that was farther from the Earth than Polar. On the other hand, the higher speed for the second event may be supported by the faster and stronger interplanetary shock actuating along the magnetopause. Also we note here

Satellite	X [Re]	Y [Re]	Z [Re]	Arrival Time, UT	Region
SOHO	241.3	-82.0	14.3	1642:36	SW
ACE	229.9	40.9	-17.0	1648:10	SW
Genesis	186.9	-1.5	-1.5	1659:00	SW
Wind	96.4	-29.9	5.5	1724:49	SW
Geotail	18.55	8.13	1.92	1747:50	SW
GOES–8	6.06	1.25	2.32	1750:34	MS
GOES–10	4.62	-4.72	0.06	1750:38	MS
Polar	-5.9	6.0	1.7	1752:50	MS
Cluster SC1	-8.60	13.8	4.43	1753:30	MS
-	11.4	-1.2	0.6	1749:29	MP

Table 1: Satellite locations in GSE coordinates and arrival times/compression onsets for the first shock on November 9, 2002. The last line shows the estimated arrival of the IP shock to the magnetopause. SW — solar wind, MS — magnetosphere.

Satellite	X [Re]	Y [Re]	Z [Re]	Arrival Time, UT	Region
SOHO	241.2	-82.1	14.2	1755:56	SW
ACE	229.9	41.0	-17.0	1754:12	SW
Genesis	186.9	-1.5	-1.5	1807:00	SW
Wind	96.6	-29.9	5.5	1827:49	SW
Geotail	17.76	8.63	1.76	1846:08	SW
GOES–8	5.41	2.8	2.56	1849:07	MS
GOES–10	5.57	-3.48	0.73	1849:13	MS
Polar	-5.55	5.2	2.2	1850:40	MS
Cluster SC1	-8.62	14.34	3.93	1851:00	MS
-	9.4	0.3	-1.9	1848:29	MP

Table 2: Satellite locations in GSE coordinates and arrival times/compression onsets for the second shock on November 9, 2002. The estimated arrival of the shock to the magnetopause in the last line. SW — solar wind, MS — magnetosphere.

that a significant distortion of the wave front was expected near the flank magnetopause.

Both shock fronts at Geotail (in both cases first panels of Figures 6a,b) last about 10 s. From the high-resolution data, two parts of the fronts on the GOES spacecraft can be distinguished. First, there are slow 3–5 min. long ramps, already reported elsewhere. On top, at the beginning of them, there are very fast step-like fronts taking about one half of the total field compression. They last about 10 s — the same time as the original shock fronts seen in the solar wind by Geotail, and they are mainly caused by the increase of the H_p (northward) component at GOES–8. A small decrease of the magnitude follows after this fast front, similarly as in the simulation case 1 by Guo et al. [2005]. The second part of fronts starts by a steep (~ 30 s) decrease of the H_e (earthward) component and continuing increase of the H_p component. No such double-part structure is seen in the Geotail data, which was upstream the bow shock in the solar wind. The last panel in Figure 6 shows magnetic field magnitudes from the Cluster spacecraft. During the first event, the Cluster fleet saw large fluctuations of the magnetic field magnitude. At the moment of the passage of the disturbance after 1753 UT, their frequency increased and the first leading front is quite fast (about 30 s, not resolved at SC2). During the second

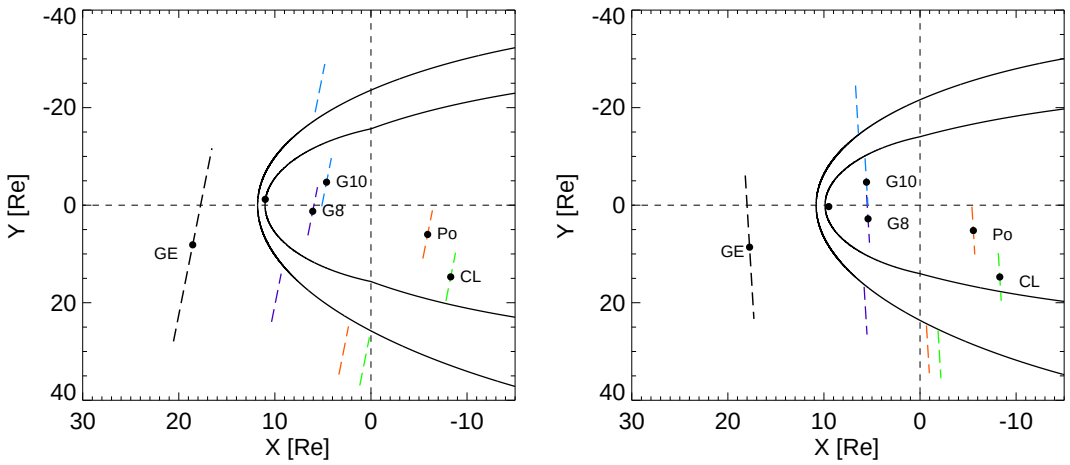

Figure 5: (a) Positions of satellites for the first case on November 9, 2002. Comparison of propagation of disturbance in the Earth's magnetosphere and propagation of original shock in the solar wind. Dashed lines in the magnetosphere depict observations of disturbance. Dashed lines in the solar wind depict the shock, if we suggest the same speed and shape of both shocks in the solar wind. (b) Similar situation for the second case.

event (after 1852 UT), a wide ramp is seen by all Cluster spacecraft lasting up to 7 minute (at SC2).

For the reported events, GOES measurements revealed very fast fronts of the magnetic field compression (about 10 s), comparable with the interplanetary shock front duration in the solar wind, followed by another slower compression and rotation of the magnetic field. Russell et al. [1999] explained a similar fast front observation by forming shock–like features due to slowing of compressional waves below the speed of IPS in the denser inner magnetosphere. Other proposed explanations, taking into account the front structure, are:

1. Observation of the original shock in magnetosphere is followed by a reverse going rarefaction wave reflected from the denser plasmasphere (supported by numerical simulations by Guo et al. [2005], Ridley et al. [2006]). On the other hand, Samsonov et al. [2007] supported the reflection of IP shock at ionosphere rather than at plasmasphere.

2. A double part structure is created during the interaction of IPS with the BS/MP system and swept into the magnetosphere. Similar double-step profiles of the density and magnetic field of IPS in the magnetosheath were already reported, e.g., by Samsonov et al. [2006] and Šafránková et al. [2007a], but timing related to different propagation speeds would have to be verified. So far we were not able to find simultaneous multipoint observations in the magnetosheath and at the geostationary orbit with sufficient time resolution for such study.

Global MHD simulation

To verify our experimental investigation, we used the numerical MHD models to model the November 9, 2002 events. Simulations enable us to discuss the processes inside the

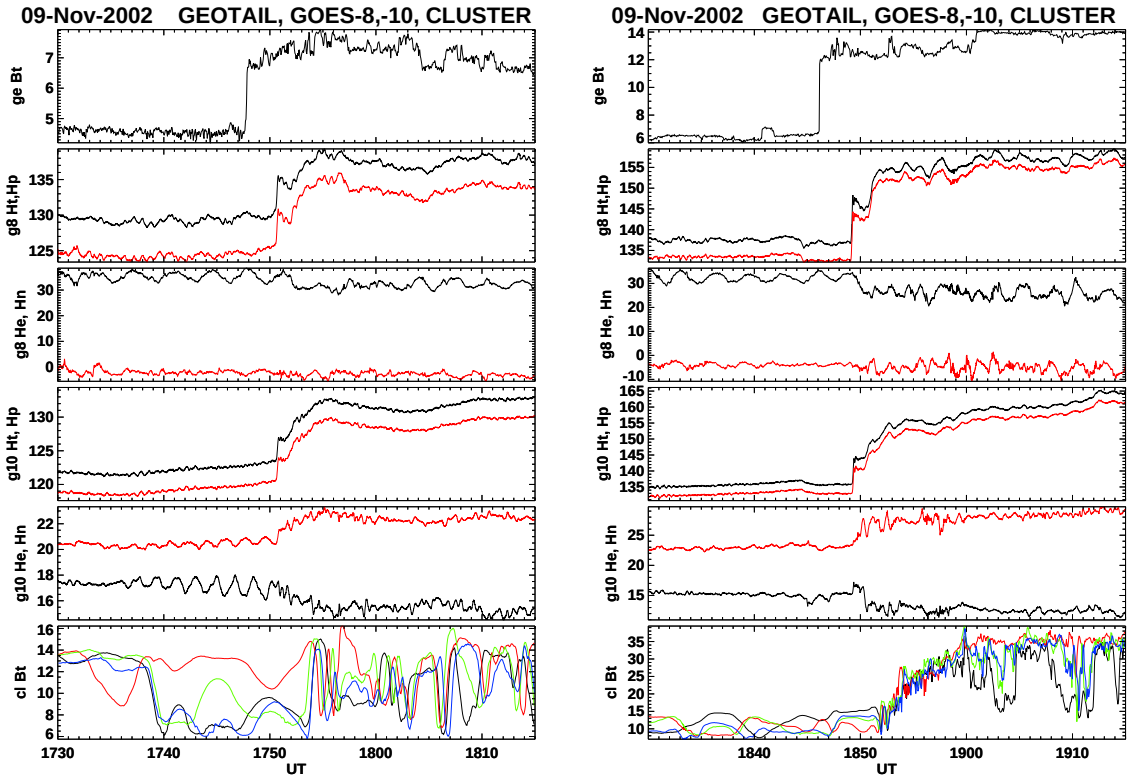

(a) (b)

Figure 6: November 9, 2002 events in detail. (a) Shock at 1750 UT, (b) Shock at 1850 UT. The top panels show the magnitude of IMF as measured by Geotail. The next two panel pairs depict the GOES–8 and GOES–10 high-resolution magnetic field data in local S/C coordinates (H_t magnitude, H_p northward component (in grey), H_e earthward component, H_n normal to both H_p and H_e, eastward (in grey)). The bottom panels plot the magnitude of magnetic fields measured by Cluster SC1 (black), SC2, SC3, and SC4 (grey). All panels in nT units.

magnetosphere and to trace the disturbance propagation and to directly compare observations with predictions.

The first selected GUMICS-4 code [Janhunen, 1996, Grand Unified Magnetosphere - Ionosphere Coupling simulation,] is a global MHD simulation coupled with a comprehensive ionospheric model developed and run at Finnish Meteorological Institute. It consists of two parts: MHD magnetospheric part and electrostatic ionospheric part.

The GUMICS-4 global MHD code solves the ideal MHD equations to provide the self-consistent temporal and spatial evolutions of the plasma in the magnetosphere and in the solar wind. The simulation box ranges from 32 R_E upstream of the Earth to -224 R_E in the tailward direction and $\pm$64 R_E in the directions perpendicular to the Sun-Earth line. The equations are solved in the geocentric solar ecliptic (GSE) coordinates. The finest grid resolution is 1/4 R_E whenever the code detects large spatial gradients.

The second selected tool is the 3D global BATS-R-US code (Block-Adaptive-Tree-Solar wind-Roe-Upwind-Scheme) described by Groth et al. [2000], provided by CCMC (Community Coordinated Modeling Center) and run at web-site http://ccmc.gsfc.nasa.

gov/index.php. The Space Weather Modeling Framework (BATS-R-US with Rice Convection Model) contains 9 modules that cover the various regions between the Sun and Earth. We have used the Global Magnetosphere (GM) module which describes the Earth's magnetosphere and is driven by upstream satellite data (Wind). The GM module includes the magnetosphere from 33 R_E upstream to some 250 R_E downtail. The GM module has a near-Earth boundary located between 2.5 and 3.5 R_E distance from the center of the Earth. Near-Earth boundary conditions are determined by the interaction with the Inner Magnetosphere (IM) module. The IM module obtains the information on closed field lines from GM and the electrostatic potential from the Ionospheric Electrodynamics module and provides density and pressure corrections back to GM. The finest grid resolution is 1/4 R_E around the Earth or in the dayside magnetosphere.

Comparison of observation with GUMICS-4

While in the solar wind, the shock fronts lasted for about 10 s, disturbance fronts in the dayside magnetosphere showed slower compression, and lasted for about 5 min. The simulation produced disturbance fronts, which lasted about 6 minutes. As it was mentioned above, the solar wind shock speeds from the real data were calculated to be about 392 km/s for the first case and about 425 km/s for the second one. Calculated GUMICS-4 shock speeds were about 360 and 420 km/s, Table 3. Timing of the real observations and simulation is summarized in Table 4. The simulation showed disturbance passages with a time delay about 140 s for the first event and about 60 s for the second event.

Disturbance	**Event 1**		**Event 2**	
	Obs. data	**GUMICS-4**	**Obs. data**	**GUMICS-4**
v_{sw}	324	-	348	-
$v_{sh}(SW)$	380	360	425	420
Uncertainty	$\pm$ 10	$\pm$ 20	$\pm$ 10	$\pm$ 20
$v_{ms}(D)$	550	390	671	425
$v_{ms}(D-N)$	588	500	745	570
$v_{ms}(N)$	588	410	776	780
Uncertainty	$\pm$ 50	$\pm$ 85	$\pm$ 50	$\pm$ 85

Table 3: November 9, 2002 interplanetary shock event: Propagation speeds in the solar wind and in the magnetosphere: v_{sw} is the solar wind speed, v_{sh} is the shock speed in the solar wind, v_{ms} is the disturbance speed in the magnetosphere, where D denotes dayside values, N nightside value and D-N means trans-terminator ("central") values. Speeds determined from observations are shown in the left columns, while those determined from the GUMICS-4 global MHD simulation are shown in the right columns for the two events separately.

GOES-8 and GOES-10 satellites observed magnetic field compressions but there are no plasma measurements on these spacecraft. Polar observed mainly a density compression and almost no magnetic field compression. Apart from the magnetic field compression, Cluster observed also density compression, fluctuations in velocity, and ion deflection (tailward). During simulation, at the position of the real satellites (GOES-8, 10) we found magnetic field and density compression. At the position of Polar, the simulated

Satellite	Observation	GUMICS-4
GOES-8	1750:41, 1849:12 UT	1753:00, 1850:30 UT
GOES-10	1750:44, 1849:16 UT	1753:00, 1850:00 UT
Polar	1752:50, 1850:40 UT	1756:00, 1853:30 UT
Cluster-1	1753:20, 1852:10 UT	1755:30, 1853:00 UT

Table 4: Observation times for both events as compared to MHD simulation GUMICS-4.

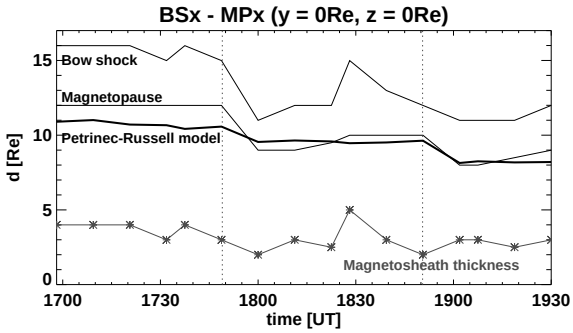

Figure 7: November 9, 2002 interplanetary shock event simulation: Magnetopause and bow shock distances from the Earth in R_E. The grey line shows the magnetosheath thickness along the Sun-Earth line. The thick black line shows the magnetopause position derived from the Petrinec and Russell model of the magnetopause using the Wind satellite data.

data showed mainly a density compression. And at the position of Cluster except density compression, there was also a weak magnetic field compression.

According to the simulation, after interaction with FFS, the magnetopause starts to move earthward with the speed of about 30 km/s for both cases. First FFS reaches the magnetopause at time 1750 UT, the second FFS at time 1850 UT. In the second case, the magnetosphere was more compressed, the main reason being the higher solar wind shock speed in this case. From the density gradient and magnetic field we detected positions of the dayside magnetopause and dayside bow shock in the simulation results. They are shown in Figure 7, where we depict the positions of the structures at the nose of the magnetosphere because FFS propagated almost perpendicularly to the Sun-Earth line. The bow shock reacts mainly to changes of the solar wind conditions, magnetic field, and dynamic pressure. Magnetopause interacts with the FFS.

Figure 8 illustrates the strong compression of the magnetosphere during both shock passages. According to the simulation, the bow shock moves from near 16 to near 13 R_E during the first event, and from near 15 to near 12 R_E during the second event, see Figure 7. The magnetopause compression was not axially symmetric with respect to the Sun-Earth line; during both events, the compression was stronger in the low latitudes than near the polar regions.

Figure 9 shows that the Polar satellite was located in the enhanced plasma flow during both events. During the first event, Polar observed a slower increase of the plasma density, which can be interpreted as Polar being at the edge of the plasma flow. During the disturbance passages, the plasma flow crossed over the satellite and was seen as an intensification of the flow speeds at that location. During the second event, the plasma flow

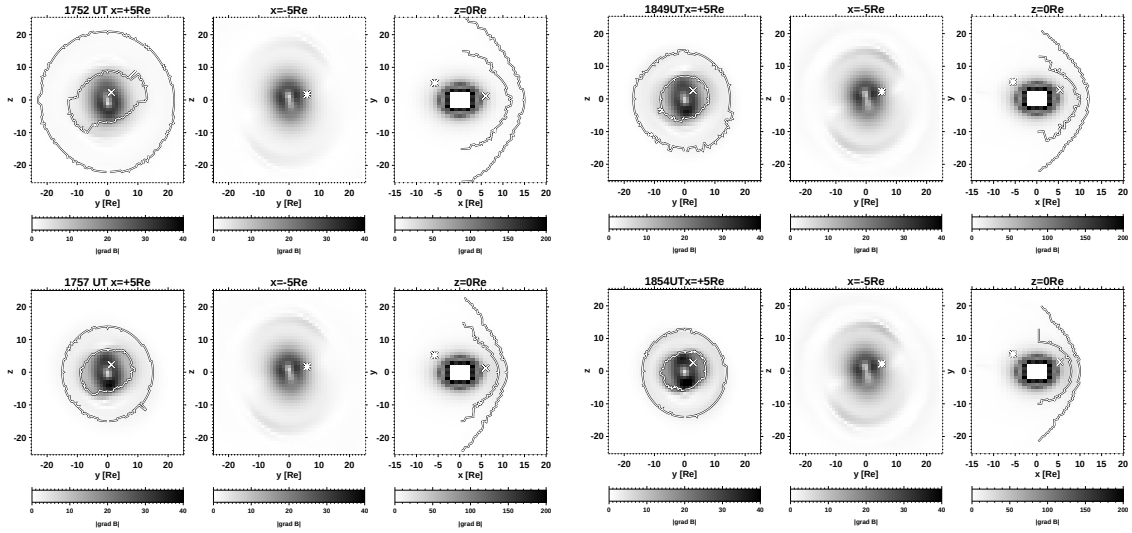

(a) (b)

Figure 8: (a) November 9, 2002 interplanetary shock Event 1 simulation: A cross-section of the magnetosphere in the YZ-plane at X = 5 R_E (left), X = -5 R_E (middle), and in the equatorial plane (right) at Z = 0 R_E at 1752 UT (top row) and 1757 UT (bottom row). The grey coding shows magnitudes of the magnetic field gradient in nT$/R_E$. The black and white lines in the left and right panels show the positions of the bow shock and the magnetopause. The position of GOES-8 and Polar are shown with the black and white cross and asterisk, respectively. (b) November 9, 2002 interplanetary shock Event 2 simulation: magnitudes of the magnetic field gradient in nT$/R_E$ in a format similar to panel (a) at 1849 UT (top row) and 1854 UT (bottom row).

was stronger and closer to the Earth, which was caused by an already more compressed magnetosphere after the first disturbance passage.

Figure 10 demonstrates that the disturbance front does not stay planar in the magnetosphere. Similarly, recent global MHD simulations [Ridley et al., 2006] have also shown a significant deformation of the interplanetary shock front in the magnetosphere. The normals of both IP shocks are not strictly parallel to the Sun-Earth line and this induces an asymmetry to the disturbance propagation across the magnetosphere as it is demonstrated in Figure 10. It displays the disturbance propagation in the equatorial plane using time derivatives of the magnetic field. The compression of the magnetic field is a little stronger in the dayside magnetosphere adjacent to the interplanetary shock front. The disturbance wavefront is slightly faster on the opposite side of the magnetosphere (both dayside and nightside) where the wavefront normal is closer to the original shock propagation direction.

Comparison of GUMICS-4 with BATS-R-US

To compare the real observation and to verify the GUMICS-4 simulation, we performed also simulation of those events using the 3D global BATS-R-US model, Figure 11.

In the GUMICS-4 simulation, we used data from Geotail, which was located in front of the Earth's bow shock, as the solar wind input. The BATS-R-US simulation used Wind

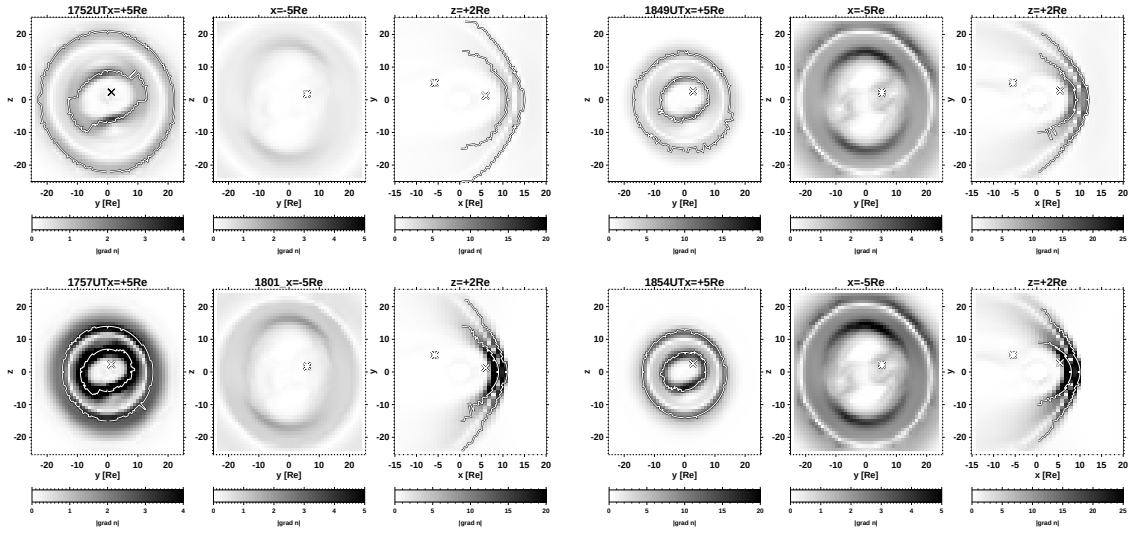

(a) (b)

Figure 9: (a) November 9, 2002 interplanetary shock Event 1 simulation: A cross-section of the magnetosphere in the YZ-plane at X = 5 R_E (left), X = -5 R_E (middle), and in the equatorial plane (right) at Z = +2 R_E at 1752 UT (top row) and 1757 UT (bottom row). The grey coding shows magnitudes of the plasma density gradient in cm^{-3}/R_E in the given plane. Other description - see Figure 8. (b) November 9, 2002 interplanetary shock Event 2 simulation: magnitudes of the plasma density gradient in cm^{-3}/R_E in a format similar to panel (a) at 1849 UT (top row) and 1854 UT (bottom row).

data instead, propagated to the simulation box entry side.

Figure 11 brings the magnetic field and plasma density comparison of both simulations with the real observation of the GOES-8 satellite position. At the beginning both simulations observed lower values of the magnetic field (about 10 nT), however, they attained the same level as real observations after the first shock passage. GUMICS-4 observed larger fluctuations about $\pm$ 10 nT. We have no plasma density observation from GOES satellites. GUMICS-4 observed lower values of the plasma density (from 1.5 cm^{-3} to 10 cm^{-3}) than the BATS-R-US (from 20 cm^{-3} to 25 cm^{-3}) simulation. Both simulations showed similar plasma density profiles. During the first disturbance passage, they saw almost no change in the plasma density. The second event appears that there was stronger plasma compression.

The shock fronts lasted about 30 s in the solar wind, however, in the Earth's magnetosphere, the disturbance fronts lasted about 5 min (GOES-8 and 10), with remark to the fast initial part according to high time resolution data. Simulation BATS-T-US reveals also 5 minutes, simulation GUMICS-4 reveals 7 minutes for the first event, for the second event also 5 minutes. The first passage was observed in the same time according to the BATS-R-US simulation and the GOES-8 satellite observation. GUMICS-4 had 2-minute time delay. In the second case, both simulations showed the same 1-minute time delay here.

Magnetopause positions are compared in Figure 12. The BATS-R-US magnetopause position (thick dashed grey line) corresponded mainly to the Petrinec and Russell model. The GUMICS-4 magnetopause position stayed stable till the first moment of the interac-

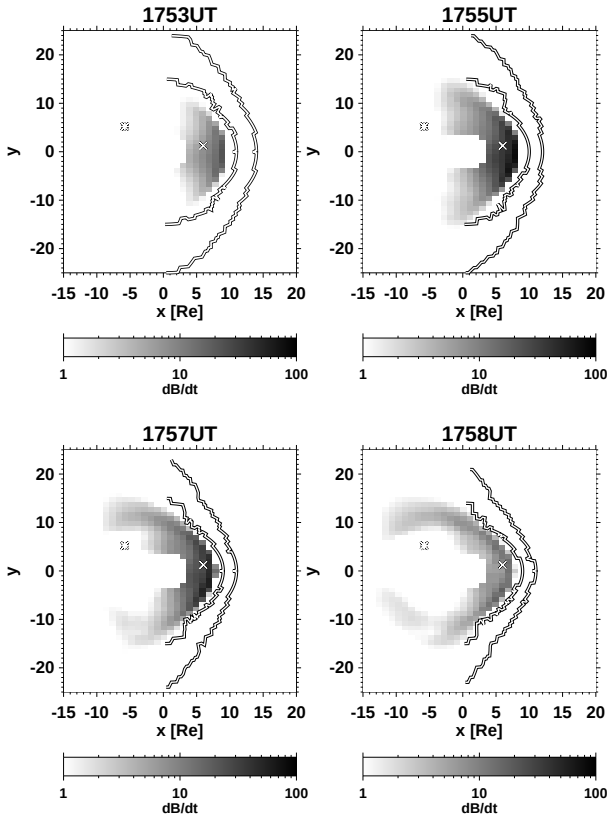

Figure 10: November 9, 2002 interplanetary shock Event 1: the disturbance propagation in the equatorial plane using time derivatives of magnetic field in four times: 1753, 1755, 1757, and 1758 UT. The grey scale is in nT/min.

tion of magnetopause with the IP shock.

Currently the BATS-R-US tool allows a slightly better time resolution of the simulation than GUMICS-4. Both models cannot perform the exact simulation of real events, as they need to set $B_X = 0$ at the solar wind input. Also they enter the same solar wind input conditions at the whole simulation box entry side. Because of that it was not possible to simulate oblique structures in the solar wind like CIR driven shocks and other similar phenomena. The MHD model by Samsonov is supposed to be soon ready to perform simulations of this kind (personal communication).

Conclusion

The main part of the thesis concentrates on the analysis and simulation of a fast forward shock in the solar wind and its evolution through the magnetosheath to the inner magnetosphere.

In our statistical study [Andreeova and Prech, 2007b] and [Andreeova and Prech, 2007a][A1] based on 42 events registered during 1997-2006 years we have investigated the propagation of IP shocks in the Earth's magnetosphere. Under assumptions of planar shocks, we calculated shock normals applying different methods [Andreeova and Prech, 2007b] and associated disturbance speeds inside the magnetosphere using a timing of various spacecraft. We obtained speeds in the range of 450-1500 km/s (consistently with

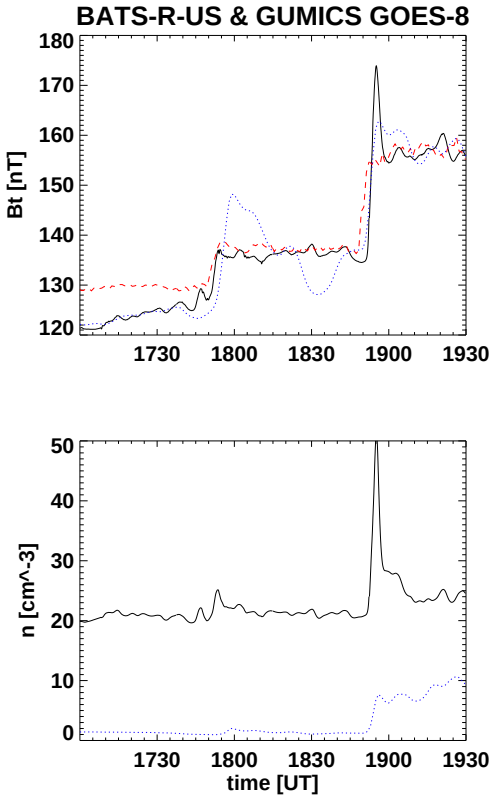

Figure 11: November 9, 2002 interplanetary shock event in position of the GOES-8 satellite: comparison of the total magnetic field and plasma density with BATS-R-US and GUMICS-4 simulations. The dashed grey line represents the GOES-8 observation, the solid black line represents the BATS-R-US simulation, and the dotted grey line represents the GUMICS-4 simulation.

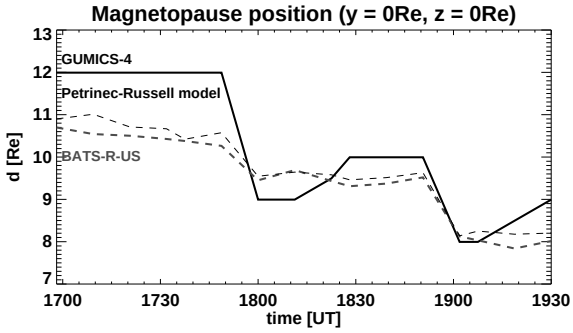

Figure 12: November 9, 2002 magnetopause position: the dashed black line shows the magnetopause position derived from the Petrinec and Russell model using the Wind satellite data, the thick dashed grey line shows the results of the BATS-R-US model, and solid black line depicts the GUMICS-4 simulation.

Nopper et al. [1982] and Wilken et al. [1982]). We showed that the disturbance speeds in the magnetosphere are higher than the original shock speed in the solar wind and that the propagation speeds gradually increase tailward from the subsolar point. Furthermore, a comparison of propagation speeds with the upstream solar wind dynamic pressure showed that these speeds are larger for higher dynamic pressure. The dependence of disturbance speeds in the magnetosphere on the southward/northward B_Z component and the IP shock compression ratios were not clear enough in our data set.

In details, we studied double fast forward shocks on November 9, 2002 using measurements of many spacecraft [Andreeova and Prech, 2007a; Andreeova et al., 2008][A1,A2]. For these two shocks, we estimated the speeds of disturbance propagation between the dayside and nightside magnetosphere to be 590 km/s and 714-741 km/s, respectively. We partially attributed this increase to higher Alfven speed in the outer magnetosphere due to the compression of the magnetosphere as a consequence of the first event, and partially to the faster and stronger driving interplanetary shock. Furthermore, high-time resolution GOES magnetic field data revealed a complex structure of the compressional wave fronts at the dayside geosynchronous orbit during these events, with initial very steep parts (10 s). We discussed their relation to the double-step profiles in the density and magnetic field during the passage of the IP shock through the magnetosheath [Šafránková et al., 2007b,a; Samsonov et al., 2006] and the model prediction of the wave reflection in the inner magnetosphere [Samsonov et al., 2007].

The observations of the November events were compared with the GUMICS-4 and BATS-R-US global MHD models [Andreeova et al., 2008][A2]. The simulation results allow us to trace the 3D propagations of the IP shock front in different regions of the magnetosphere. Using these simulations, we confirmed that the disturbance speeds in the Earth's magnetosphere were higher for the second shock due to the higher dynamic pressure. Moreover, we showed that the profile and speed changes were largest within the high-latitude magnetosheath and plasma sheet and that the front of the disturbance is significantly deformed in the magnetosphere [Andreeova et al., 2008][A2].

Acknowledgements

This work was supported by the Czech Grant Agency under contracts 202/03/H162, 147307 and partly supported by the Czech Ministry of Education through the Research Project MSH0021620860.

We thank J. C. Kasper (MIT) for providing the data and support to his interplanetary shock database, and the CDAWeb service and the corresponding PIs for the satellite data. Particularly, I would like to thank to T. I. Pulkkinen and T. V. Laitinen (FMI) for invitation to use the GUMICS-4 model and their kind support.

References

Andreeova, K., Prech, L., 2007a. Propagation of interplanetary shocks into the Earth's magnetosphere. Adv. Space Res. 40, 1871–1880, doi:10.1016/j.asr.2007.04.079.

Andreeova, K., Prech, L., 2007b. Properties of Fast Forward Shock Caused Waves in the Magnetosphere. in WDS'07 *Proceedings of Contributed Papers: Part II - Physics of*

Plasmas and Ionized Media, edited by J. Safrankova and J. Pavlu, pp. 22-28, Prague, Matfyzpress, ISBN 978-80-7378-024-1.

Andreeova, K., Pulkkinen, T. I., Laitinen, T., Prech, L., 2008. Shock propagation in the magnetosphere: Observations and MHD simulations compared. J. Geophys. Res.

Balogh, A., Dunlop, M. W., Cowley, S. W. H., Southwood, D. J., Thomlinson, J. G., Glassmeier, K. H., Musmann, G., Luhr, H., Buchert, S., Acuna, M. H., Fairfield, D. H., Slavin, J. A., Riedler, W., Schwingenschuh, K., Kivelson, M. G., 1997. The Cluster Magnetic Field Investigation. Space Sci. Rev. 79, 65–91.

Bellomo, A., Mavretic, A., 1978. Description of the MIT plasma experiment on IMP 7/8. in Rep. CSR TR-78-2, 51Cent. for Space Res., MIT, Cambridge.

Berdichevsky, D. B., Szabo, A., Lepping, R. P., Vinas, A. F., Mariani, F., 2000. Interplanetary fast shocks and associated drivers observed through the 23rd solar minimum by Wind over its first 2.5 years. J. Geophys. Res. 105, 27289–27314.

Grib, S. A., 1982. Interaction of non-perpendicular/parallel solar wind shock waves with the Earth's magnetosphere. Space Sci. Rev. 32, 43–48.

Grib, S. A., Briunelli, B. E., Dryer, M., Shen, W.-W., 1979. Interaction of interplanetary shock waves with the bow shock-magnetopause system. J. Geophys. Res. 84, 5907–5921.

Groth, C. P. T., De Zeeuw, D. L., Gombosi, T. I., Powell, K. G., 2000. Global three-dimensional MHD simulation of a space weather event: CME formation, interplanetary propagation, and interaction with the magnetosphere. J. Geophys. Res. 105, 25053–25078.

Guo, X.-C., Hu, Y.-Q., Wang, C., 2005. Earth's magnetosphere impinged by interplanetary shocks of different orientations. Chin. Phys. Lett. 22, 3221–3224.

Harvey, P., Mozer, F. S., Pankow, D., Wygant, J., Maynard, N. C., Singer, H., Sullivan, W., Anderson, P. B., Pfaff, R., Aggson, T., Pedersen, A., Fälthammar, C.-G., Tanskannen, P., Feb. 1995. The Electric Field Instrument on the Polar Satellite. Space Sci. Rev. 71, 583–596.

Ipavich, F. M., Galvin, A. B., Lasley, S. E., Paquette, J. A., Hefti, S., Reiche, K.-U., Coplan, M. A., Gloeckler, G., Bochsler, P., Hovestadt, D., Grünwaldt, H., Hilchenbach, M., Gliem, F., Axford, W. I., Balsiger, H., Bürgi, A., Geiss, J., Hsieh, K. C., Kallenbach, R., Klecker, B., Lee, M. A., Managadze, G. G., Marsch, E., Möbius, E., Neugebauer, M., Scholer, M., Verigin, M. I., Wilken, B., Wurz, P., 1998. Solar wind measurements with SOHO: The CELIAS/MTOF proton monitor. J. Geophys. Res. 103, 17205–17214.

Janhunen, P., 1996. GUMICS-3 A Global Ionosphere-Magnetosphere Coupling Simulation with High Ionospheric Resolution. In: Guyenne, T.-D., Hilgers, A. (Eds.), Environment Modeling for Space-Based Applications. Vol. 392 of ESA Special Publication. pp. 233–+.

Kasper, J. C., 2005. Interplanetary shock database from WIND satellite.
URL `http://space.mit.edu/home/jck/shockdb/shockdb.htm`

Klimov, S., Romanov, S., Amata, E., Blecki, J., Büchner, J., Juchniewicz, J., Rustenbach, J., Triska, P., Woolliscroft, L. J. C., Savin, S., Afanas'yev, Y., de Angelis, U., Auster, U., Bellucci, G., Best, A., Farnik, F., Formisano, V., Gough, P., Grard, R., Grushin, V., Haerendel, G., Ivchenko, V., Korepanov, V., Lehmann, H., Nikutowski, B., Nozdrachev, M., Orsini, S., Parrot, M., Petrukovich, A., Rauch, J. L., Sauer, K., Skalsky, A., Slominski, J., Trotignon, J. G., Vojta, J., Wronowski, R., 1997. ASPI experiment: measurements of fields and waves on board the INTERBALL-1 spacecraft. Annales

Geophysicae 15, 514–527.
Kokubun, S., Yamamoto, T., Acuna, M. H., Hayashi, K., Shiokawa, K., Kawano, H., 1994. The Geotail Magnetic Field Experiment. J. Geomag. Geoelectr. 46, 7–21.
Koval, A., Šafránková, J., Němeček, Z., Přech, L., Samsonov, A. A., Richardson, J. D., 2005. Deformation of interplanetary shock fronts in the magnetosheath. Geophys. Res. Let. 32, L15101, doi:10.1029/2005GL023009.
Koval, A., Šafránková, J., Němeček, Z., Samsonov, A. A., Přech, L., Richardson, J. D., Hayosh, M., 2006. Interplanetary shock in the magnetosheath: Comparison of experimental data with MHD modeling. Geophys. Res. Let. 33, L11102, doi:10.1029/2006GL025707.
Lepping, R. P., Acũna, M. H., Burlaga, L. F., Farrell, W. M., Slavin, J. A., Schatten, K. H., Mariani, F., Ness, N. F., Neubauer, F. M., Whang, Y. C., Byrnes, J. B., Kennon, R. S., Panetta, P. V., Scheifele, J., Worley, E. M., 1995. The Wind Magnetic Field Investigation. Space Sci. Rev. 71, 207–229.
Lin, R. P., Anderson, K. A., Ashford, S., Carlson, C., Curtis, D., Ergun, R., Larson, D., McFadden, J., McCarthy, M., Parks, G. K., Rème, H., Bosqued, J. M., Coutelier, J., Cotin, F., D'Uston, C., Wenzel, K.-P., Sanderson, T. R., Henrion, J., Ronnet, J. C., Paschmann, G., 1995. A Three-Dimensional Plasma and Energetic Particle Investigation for the Wind Spacecraft. Space Sci. Rev. 71, 125–153.
McComas, D. J., Bame, S. J., Barker, P., Feldman, W. C., Phillips, J. L., Riley, P., Griffee, J. W., 1998. Solar Wind Electron Proton Alpha Monitor (SWEPAM) for the Advanced Composition Explorer. Space Sci. Rev. 86, 563–612.
Mukai, T., Machida, S., Saito, Y., Hirahara, M., Terasawa, T., Kaya, N., Obara, T., Ejiri, M., A., N., 1994. The low energy particle (LEP) experiment onboard the Geotail satellite. J. Geomagn. Geoelectr. 46, 669–692.
Nopper, Jr., R. W., Hughes, W. J., Maclennan, C. G., McPherron, R. L., 1982. Impulse-excited pulsations during the July 29, 1977, event. J. Geophys. Res. 87, 5911–5916.
Nozdrachev, M. N., Skalsky, A. A., Styazhkin, V. A., Petrov, V. G., 1998. Some Results of Magnetic Field Measurements by the FM-3I Flux-Gate Instrument Onboard the INTERBALL-1 Spacecraft. Cosmic Research 36, 251–+.
Ogilvie, K. W., Chornay, D. J., Fritzenreiter, R. J., Hunsaker, F., Keller, J., Lobell, J., Miller, G., Scudder, J. D., Sittler, Jr., E. C., Torbert, R. B., Bodet, D., Needell, G., Lazarus, A. J., Steinberg, J. T., Tappan, J. H., Mavretic, A., Gergin, E., 1995. SWE, A Comprehensive Plasma Instrument for the Wind Spacecraft. Space Sci. Rev 71, 55–77.
Prech, L., Safrankova, J., Nemecek, Z., 2008. Response of magnetospheric boundaries to the interplanetary shock: Themis contribution. Geophys. Res. Lett. 35, L17S02, doi:10.1029/2008GL033593.
Reme, H., Bosqued, J. M., Sauvaud, J. A., Cros, A., Dandouras, J., Aoustin, C., Bouyssou, J., Camus, T., Cuvilo, J., Martz, C., Medale, J. L., Perrier, H., Romefort, D., Rouzaud, J., D'Uston, C., Mobius, E., Crocker, K., Granoff, M., Kistler, L. M., Popecki, M., Hovestadt, D., Klecker, B., Paschmann, G., Scholer, M., Carlson, C. W., Curtis, D. W., Lin, R. P., McFadden, J. P., Formisano, V., Amata, E., Bavassano-Cattaneo, M. B., Baldetti, P., Belluci, G., Bruno, R., Chionchio, G., di Lellis, A., Shelley, E. G., Ghielmetti, A. G., Lennartsson, W., Korth, A., Rosenbauer, H., Lundin, R., Olsen, S., Parks, G. K., McCarthy, M., Balsiger, H., 1997. The Cluster Ion Spectrometry (cis) Experiment. Space Sci. Rev. 79, 303–350.
Ridley, A. J., De Zeeuw, D. L., Manchester, W. B., Hansen, K. C., 2006. The magnetospheric and ionospheric response to a very strong interplanetary shock and coronal

mass ejection. Adv. Space Res. 38, 263–272.
Russell, C. T., Snare, R. C., Means, J. D., Pierce, D., Dearborn, D., Larson, M., Barr, G., Le, G., 1995. The GGS/POLAR magnetic fields investigation. Space Sci. Rev. 71, 563–582.
Russell, C. T., Zhou, X. W., Chi, P. J., Kawano, H., Moore, T. E., Peterson, W. K., Cladis, J. B., Singer, H. J., 1999. Sudden compression of the outer magnetosphere associated with an ionospheric mass ejection. Geophys. Res. Let. 26, 2343–2346.
Safrankova, J., Zastenker, G., Nemecek, Z., Fedorov, A., Simersky, M., Prech, L., May 1997. Small scale observation of magnetopause motion: preliminary results of the INTERBALL project. Annales Geophysicae 15, 562–569.
Samsonov, A. A., Němeček, Z., Šafránková, 2006. Numerical MHD modeling of propagation of interplanetary shock through the magnetosheath. J. Geophys. Res. 111, A08210, doi:10.1029/2005JA011537.
Samsonov, A. A., Sibeck, D. G., Imber, J., 2007. MHD simulation for the interaction of an interplanetary shock with the Earth's magnetosphere. J. Geophys. Res. 112, A12220, doi:10.1029/2007JA012627.
Singer, H. J., Matheson, L., Grubb, R., Newman, A., Bouwer, S. D., 1996. Monitoring space weather with the GEOS magnetometers. SPIE conference proceedings, GEOS-8 and Beyond 2812, 299–308.
Smith, C. W., L'Heureux, J., Ness, N. F., Acuña, M. H., Burlaga, L. F., Scheifele, J., Jul. 1998. The ACE Magnetic Fields Experiment. Space Sci. Rev. 86, 613–632.
SOHO, 2007. Interplanetary shocks and other interesting events from SOHO satellite. URL `http://umtof.umd.edu/pm/figs.html`
Spreiter, J. R., Stahara, S. S., 1994. Gasdynamic and magnetohydrodynamic modeling of the magnetosheath: A tutorial. Adv. Space Res. 14, 5–19.
Tamao, T., 1964. The structure of three-dimensional hydromagnetic waves in a uniform cold plasma. J. Geomagn. Geoelectr. 18, 89–114.
Šafránková, J., Němeček, Z., Přech, L., Samsonov, A. A., Koval, A., Andréeová, K., 2007b. Interaction of interplanetary shocks with the bow shock. Planet. Space Sci. 55, 2324–2329.
Šafránková, J., Němeček, Z., Přech, L., Samsonov, A. A., Koval, A., Andréeová, K., 2007a. Modification of interplanetary shocks near the bow shock and through the magnetosheath. J. Geophys. Res. 112, 8212–+.
Villante, U., Lepidi, S., Francia, P., Bruno, T., 2004. Some aspects of the interaction of interplanetary shocks with the Earth's magnetosphere: an estimate of the propagation time through the magnetosheath. J. Atm. Solar-Terr. Phys. 66, 337–341.
Wilken, B., Goertz, C. K., Baker, D. N., Higbie, P. R., Fritz, T. A., 1982. The SSC on July 29, 1977 and its propagation within the magnetosphere. J. Geophys. Res. 87, 5901–5910.
Yan, M., Lee, L. C., 1996. Interaction of interplanetary shocks and rotational discontinuities with the Earth's bow shock. J. Geophys. Res. 101, 4835–4848.
Zhuang, H. C., Russell, C. T., Smith, E. J., Gosling, J. T., 1981. Three-dimensional interaction of interplanetary shock waves with the bow shock and magnetopause - A comparison of theory with ISEE observations. J. Geophys. Res. 86, 5590–5600.

Papers included in the thesis

A1 Andreeova, K., L. Prech (2007), Propagation of interplanetary shocks into the Earths magnetosphere, *Adv. Space Res.*, 40, 1871-1880, doi:10.1016/j.asr.2007.04 .079.

A2 Andreeova, K., T. I. Pulkkinen, T. V. Laitinen, L. Prech (2008), Interaction of Interplanetary Shocks with the Earth's Magnetosphere: Observations and Global MHD Simulations Compared During the Nov 9, 2002 Event, accepted to *J. Geophys. Res.*, doi:10.1029/2008JA013350.

Other papers related to the topics

- Andreeova, K. (2005), Interaction between IMF discontinuities or shocks and the Earth's Bow Shock, in WDS'05 *Proceedings of Contributed Papers: Part II - Physics of Plasmas and Ionized Media*, edited by J. Safrankova, pp. 213-219, Prague, Matfyzpress, ISBN 80-86732-59-2.

- Andreeova, K., and L. Prech (2006), Propagation of interplanetary shocks into the Earth's magnetosphere, in WDS'06 *Proceedings of Contributed Papers: Part II - Physics of Plasmas and Ionized Media*, edited by J. Safrankova and J. Pavlu, pp. 7-13, Prague, Matfyzpress, ISBN 80-86732-85-1.

- Andreeova, K., and L. Prech (2007), Properties of Fast Forward Shock Caused Waves in the Magnetosphere, in WDS'07 *Proceedings of Contributed Papers: Part II - Physics of Plasmas and Ionized Media*, edited by J. Safrankova and J. Pavlu, pp. 22-28, Prague, Matfyzpress, ISBN 978-80-7378-024-1.

- Safrankova, J., Z. Nemecek, L. Prech, A. A. Samsonov, A. Koval, and K. Andreeova (2007), Interaction of interplanetary shocks with the bow shock, *Planet. Space Sci.*, 55, 2324-2329.

- Safrankova, J., Z. Nemecek, L. Prech, A. A. Samsonov, A. Koval, and K. Andreeova (2007), Modification of interplanetary shocks near the bow shock and through the magnetosheath, *J. Geophys. Res.*, 112, A08212, doi:10.1029/2007JA012503.